Structure of nanoscale polaron correlations in $La_{1.2}Sr_{1.8}Mn_2O_7$

B. J. Campbell,[1,*] R. Osborn,[1] D. N. Argyriou,[1] L. Vasiliu-Doloc,[2,3] J. F. Mitchell,[1] S. K. Sinha,[3] U. Ruett,[1] C. D. Ling,[1] Z. Islam,[2,3] and J. W. Lynn[4]

[1]*Materials Science Division, Argonne National Laboratory, Argonne, Illinois 60439*

[2]*Department of Physics, Northern Illinois University, DeKalb, Illinois 60115*

[3]*Advanced Photon Source, Argonne National Laboratory, Argonne, Illinois 60439*

[4]*NIST Center for Neutron Research, National Institute of Standards and Technology, Gaithersburg, Maryland 20899*

(Received 6 July 2001; published 11 December 2001)

A system of strongly interacting electron-lattice polarons can exhibit charge and orbital order at sufficiently high polaron concentrations. In this study, the structure of short-range polaron correlations in the layered colossal magnetoresistive perovskite manganite $La_{1.2}Sr_{1.8}Mn_2O_7$ has been determined by a crystallographic analysis of broad satellite maxima observed in diffuse x-ray and neutron-scattering data. The resulting $\mathbf{q} \approx (0.3,0,\pm 1)$ modulation is a longitudinal octahedral-stretch mode, consistent with incommensurate Jahn-Teller-coupled charge-density-wave fluctuations, that implies an unusual orbital-stripe pattern parallel to the $\langle 100 \rangle$ directions.

DOI: 10.1103/PhysRevB.65.014427 PACS number(s): 75.30.Vn, 71.30.+h, 71.38.−k, 71.45.Lr

I. INTRODUCTION

The importance of electron-phonon coupling in amplifying the colossal magnetoresistive (CMR) effect in perovskite manganites was recognized at an early stage in the theoretical work of Millis and co-workers,[1,2] who showed that the magnetic double-exchange mechanism,[3,4] which links the nearest-neighbor electron hopping rate to the degree of spin alignment, is not sufficient, by itself, to induce a metal-insulator transition. In the insulating state above T_c, the strong coupling of the Mn^{3+} e_g electrons to Jahn-Teller distortions of the MnO_6 octahedra is essential in the formation of electron-lattice polarons, which are e_g electrons that become trapped within their self-induced lattice distortions.[5] The formation of the metallic state at T_c marks the delocalization of the e_g electrons and the collapse of their polaronic lattice distortions.[6–8] If composition is expressed in terms of the Mn^{4+} ion fraction x in these Mn^{3+}/Mn^{4+} compounds (e.g., $La_{1-x}Ca_xMnO_3$ or $La_{2-2x}Sr_{1+2x}Mn_2O_7$), CMR behavior optimally occurs in the range $0.3 < x < 0.5$.

At high e_g-electron concentrations, where polarons interact via overlapping lattice-strain fields and electronic wave functions, electronic and structural correlations can develop. The case of long-range charge and orbital (C/O) order, for example, may be viewed as one type of strongly correlated polaronic limit. While long-range polaron correlations are often absent at doping levels relevant to CMR effects, recent diffuse neutron and x-ray scattering experiments have revealed the existence of short-range polaron correlations that are intimately related to the behavior of the paramagnetic insulator to ferromagnetic metal (PI-FM) transition.[8–12] In $La_{1.2}Sr_{1.8}Mn_2O_7$, we have observed broad maxima in diffuse x-ray scattering data, approximately centered at reciprocal space positions $(h \pm 0.3, k, l \pm 1)$.[8] These broad scattering maxima are diffuse surrogates of the satellite reflections that would be present if the underlying structural modulations produced by the polaron correlations were long range, and appear to be quasistatic on a 1-ps time scale.[8] Here we present a structural analysis based on the integrated intensities of a large number of these broad satellite maxima, providing a detailed description of the atomic displacements associated with the short-range polaron correlations above T_c.

II. EXPERIMENT

X-ray diffuse scattering measurements were performed using $6 \times 4 \times 1$ mm and $2 \times 2 \times 0.25$ mm single-crystal samples of $La_{1.2}Sr_{1.8}Mn_2O_7$ cleaved from the same region of a boule that was grown by the floating-zone technique. Data were collected at 115 keV at the BESSRC 11ID beamline of the Advanced Photon Source using a Bruker 6500 charge-coupled device (CCD) camera (sample to detector distance $= 2.5$ m), and at 36 keV at the SRI 1ID beamline using a Ge solid- state detector.

III. RESULTS AND DISCUSSION

The diffuse scattering data in Fig. 1 were collected at 125 K using the CCD camera. Due to the small scattering angle $(2\theta \leqslant 4.1°)$, this image represents, to a good approximation,

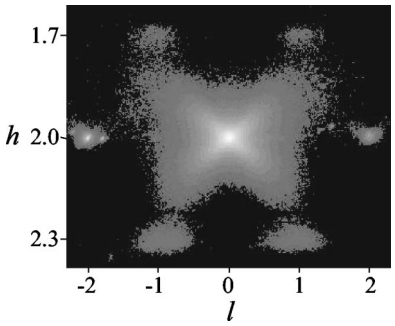

FIG. 1. Diffuse x-ray scattering data in the $k_0 = 0.005$ plane of reciprocal space simultaneously reveals polaron correlations, Huang scattering, and thermal diffuse scattering near the (200) Bragg reflection. The intensity scale of this CCD image is logarithmic, such that the strongest features are approximately 250 times more intense than the weakest features.

a constant k slice of reciprocal space centered at $(2,k_0=0.005,0)$. The "butterfly-shaped" scattering pattern at the center of the figure is associated with the strain fields induced by local Jahn-Taller (JT) distortions, and is commonly referred to as Huang scattering.[13] The two narrow peaks at $(2,k_0,\pm 2)$ are the tails of the $(2,0,\pm 2)$ Bragg peaks. Most notably, the presence of the four diffuse maxima near $(2\pm 0.3,0,\pm 1)$ indicates the presence of the short-range polaron correlations on a length scale of 10–25 Å. Although the diffuse satellites are quite broad and also several orders of magnitude weaker in intensity than the parent Bragg peaks, they are sufficiently well defined to reliably determine their integrated intensities. Because the peak widths did not vary significantly from satellite to satellite, a simple h scan through the center of each peak using the Ge solid-state detector was sufficient. The Huang scattering tails centered about nearby Bragg peaks produced a background that did vary significantly from one satellite to another. This background was accommodated by the peak fitting routine and subtracted. The intensities of 109 unique diffuse satellites were thus measured at 125 K, and used to perform a crystallographic analysis with the JANA software package.[14]

The diffuse maxima observed at positions $\mathbf{Q}\approx\mathbf{Q}_0\pm(0.3,0,\pm 1)$, where $\mathbf{Q}_0$ is a Bragg peak position associated with the parent $I4/mmm$ symmetry (i.e., $h+k+l=2n$), can be equivalently described by positions $\mathbf{Q}_0+m\mathbf{q}$, where the modulation wave vector is $\mathbf{q}\approx(0.3,0,0)$, and $\mathbf{Q}_0$ and m are further restricted by the $(3+1)$-dimensional centering condition: $h+k+l+m=2n$. It is important to note that only first-order satellite maxima (i.e., $m=\pm 1$) are observed. Thus they only appear adjacent to the $h+k+l=2n+1$ positions. This set of systematic absences leads to the selection of $Xmmm(\alpha 00)000$ as the $(3+1)$-dimensional superspace-group symmetry,[15,16] where X refers to the extended body-centering condition, $(x,y,z,t)\rightarrow(x+1/2,y+1/2,z+1/2,t+1/2)$, and implies that the modulated displacements in adjacent perovskite bilayers are 180° out of phase. In the limit of small atomic displacements, an expression for the intensities of the diffuse satellite peaks can be written as

$$I\propto|F|^2=\left|\frac{1}{2}(\mathbf{Q}_0+m\mathbf{q})\cdot\sum_n \mathbf{u}_n f_n e^{i\mathbf{Q}_0\cdot\mathbf{x}_n}\right|^2, \qquad (1)$$

where $\mathbf{x}_n$ and f_n are the position and form factor of the nth atom in the unit cell, and $\mathbf{u}_n=\mathbf{u}_c+i\mathbf{u}_s$ is the modulation amplitude vector of the nth atom, which gives the displacement of the nth atom as $\mathbf{u}_n^s\sin(\mathbf{q}\cdot\mathbf{x})+\mathbf{u}_n^c\cos(\mathbf{q}\cdot\mathbf{x})$.

After the integrated intensities were extracted and corrected for absorption, several distinct features were immediately evident. The intensities naturally separate into four distinct subsets, $(h,k)=(e,o)$, (o,e), (e,e), and (o,o), where "o" and "e" indicate odd and even integers, respectively.[17] For a given value of l, one subset is often notably more intense than the other. Because the O(3) oxygen is the only atom in the unit cell that produces a contribution to the structure factor capable of differentiating between these subsets, its displacement must be a key element of the modulation. The observed one-dimensional modulation breaks the four-fold symmetry of the average structure and splits the O(3) oxygen site into two distinct sites, referred to here as O(3a) and O(3b), where O(3a) connects two Mn atoms along the modulation direction, and O(3b) connects two Mn atoms along the direction transverse to the modulation. The intensities within each of the four subsets increase strongly with increasing h, indicating that the principal displacements are parallel to the [100] modulation direction (i.e., longitudinal). Furthermore, these intensities do not increase with k, indicating that there are no significant displacements along [010], which is also a requirement of the symmetry.

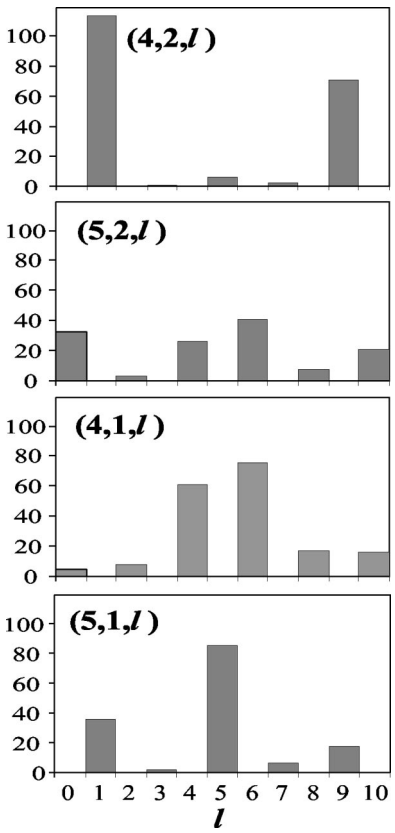

FIG. 2. A bar graph of $|F_{obs}|^2$ vs l within each of the four distinct reflection subsets. The l dependence in each example is characteristic of its subset.

Distinctive intensity trends vs l are observed within each of the four satellite subsets. The trends are roughly periodic along l with a period of roughly ten reciprocal-lattice units, a feature arising from the thickness ($\approx 2c/10$) of the perovskite bilayers. The details of this periodicity, and especially the differences amongst the four subsets, shed light on the structure of the modulation. Figure 2 contains one characteristic example from each of the four satellite subsets. By examining these variations in light of the individual contributions to Eq. (1) from each atom in the unit cell, we find that O($3a$) experiences a large longitudinal displacement that is also in phase with those of its neighbors. These observations serve as a starting model from which to refine all of the independent modulation amplitudes.

The structure in Fig. 3 illustrates the results of an $|F|^2$ refinement of the modulation amplitudes against the measured satellite intensities, which yielded an agreement factor

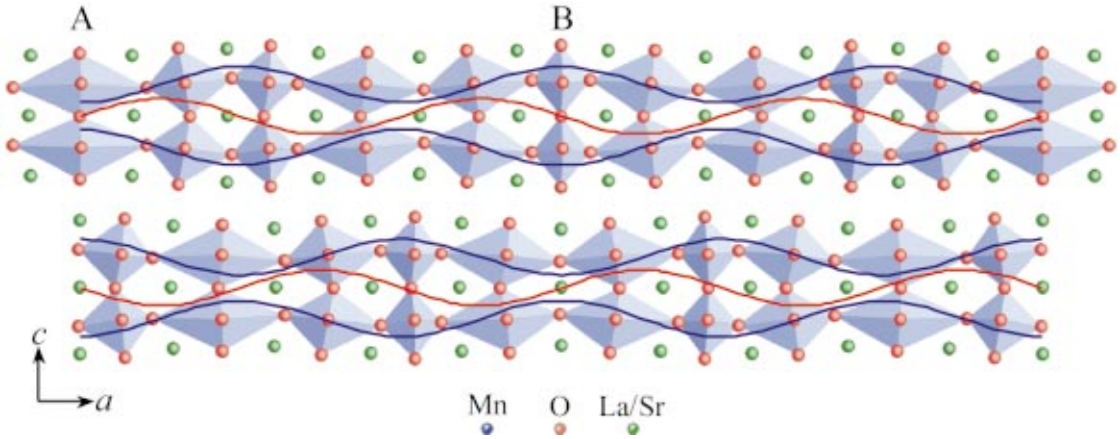

FIG. 3. (Color) Crystallographic representation of the one-dimensionally modulated structure associated with the diffuse $\mathbf{q} \approx (0.3,0,\pm 1)$ satellites. The atomic displacements are exaggerated in order to make the more subtle features of the modulation visually apparent. The directions of the atomic displacements within each perovskite sheet and bilayer follow the blue (z-component) and red (x-component) curves, where peaks indicate $+x$ or $+z$ displacements and troughs indicate $-x$ or $-z$ displacements. The incommensurate modulation period has been approximated by the commensurate value of $\frac{10}{3}$.

of $(\Sigma w_i|\triangle I_i|^2)/(\Sigma w_i I_i^2) = 16.3\%$. Only the $\mathbf{u}_x^s$ and $\mathbf{u}_z^c$ terms are permitted by symmetry,[18] and both were essential to obtaining a good fit to the measured intensities. The elongation of the Mn-O($3a$) bonds at position A in the figure is interpreted as a cooperative Jahn-Teller (JT) distortion caused by the occupation of Mn e_g orbitals with $d(3x^2-r^2)$ character. These Mn-O($3a$) bond distortions are much more pronounced than any of the others. Other cooperative features include the stacking of JT-distorted octahedra within a bilayer, the ***c*** axis compression of octahedra that experience ***a***-axis elongation, octahedral rotations about the ***b*** axis, and the 180° phase difference between the modulations in adjacent bilayers, which all appear to work together to minimize the lattice strain induced by the dominant Mn-O($3a$) distortions. After the sinusoidal modulation was applied, the model in Fig. 3 was stretched along [100] to restore the unphysically compressed octahedra at position B to their normal shapes. This stretch corresponds to a local enlargement of the [100] cell parameter within the correlated regions due to the cooperative JT distortions. Local lattice effects have been previously studied via pair distribution function analysis,[7] whereas the present analysis is only sensitive to the periodic features that produce the diffuse satellite reflections.

The red (x-component) and blue (z-component) curves in Fig. 3 illustrate the relative phases of the modulation within each perovskite sheet and bilayer. The curves are fixed by symmetry, and indicate that the ***c***-axis displacements within the two sheets of a perovskite bilayer are equal and opposite, whereas these two sheets share the same ***c***-axis displacements. This structural nuance is qualitatively similar to one proposed by Kubota *et al.*,[9] based on single-crystal neutron diffuse scattering data from the related $x = 45\%$ system. The refined values of the independent modulation amplitude components are listed in Table I in reciprocal-lattice units, together with their respective atomic coordinates.[19] Since the amplitudes in Table I all have the same relative signs, a very important feature that is not dictated by symmetry, these curves also represent the cooperative displacement directions of all of the atoms in their respective layers at each point along the modulation. Note that because the refinement scale factor is directly correlated to the modulation amplitudes in Eq. (1), the values in Table I are defined only to within an overall scale factor, which was set by assuming a maximum Mn-O bond length distortion ($\triangle_{\text{Mn-O}(3a)}$) of 0.05 Å, a reasonable value based on the JT-distorted bond lengths observed for CE-type C/O order[20,21] in $LaSr_2Mn_2O_7$.

The image in Fig. 4 represents the displacement-displacement correlation function associated with the short-range $\mathbf{q} \approx (0.3,0,\pm 1)$ modulation within a single perovskite sheet. Thus if the MnO_6 octahedron at the origin of the figure is Jahn-Teller distorted, the probability that another MnO_6 octahedron is similarly distorted will oscillate within the sheet along the modulation direction, and approach zero with increasing distance from the origin due to the finite range of the correlations. When viewed in this fashion, the smoothly varying pattern of orbital stripes that forms perpendicular to the modulation direction is readily apparent. However, one must note that the distribution in Fig. 4 is a purely statistical statement about the average size and shape of the correlated regions, rather than a picture of an individual correlated region.

The modulation illustrated in Fig. 3 challenges our current understanding of C/O order in CMR manganites. First, it

TABLE I. Average atomic coordinates (Ref. 19) and $\mathbf{q} \approx (0.3,0,\pm 1)$ modulation amplitudes.

Atom	x	y	z	$\mathbf{u}_x^s$(Å$\times 10^2$)	$\mathbf{u}_z^c$(Å$\times 10^2$)
Mn	0	0	0.0965	1.29(3)	−1.03(12)
O(1)	0	0	0	2.87(30)	
O(2)	0	0	0.1960	0.44(19)	−1.13(31)
O($3a$)	0.5	0	0.0952	4.69(20)	−1.73(35)
O($3b$)	0	0.5	0.0952	1.56(13)	−0.13(34)
La/Sr(1)	0.5	0.5	0	1.31(2)	
La/Sr(2)	0.5	0.5	0.1825	0.81(2)	−1.54(45)

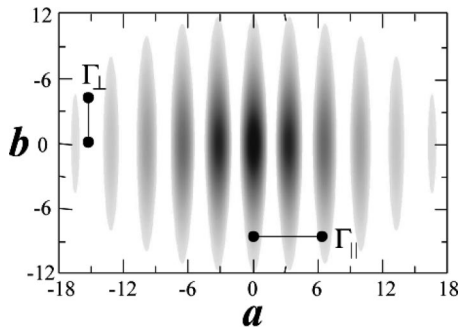

FIG. 4. The displacement-displacement correlation function associated with the short-range $\mathbf{q}\approx(0.3,0,\pm1)$ modulation within a single perovskite plane, which takes into account the wave vector and the finite widths of the diffuse satellite peaks, and consists of a $\cos^2(\mathbf{q}\cdot\mathbf{r}/2)$ modulation factor multiplied by an exponential envelope, with half width at half maximum (HWHM) values defined by the three independent correlation lengths ($\Gamma_{||}\approx 6a, \Gamma_\perp \approx 4a, \Gamma_c \approx c/2$). Dark regions indicate high probability and light regions indicate low probability. The correlated regions are large enough to encompass several stripe like periods along [100].

represents an orbital-stripe pattern parallel to the $\langle 100\rangle$ directions, and may be thought of as longitudinally modulated ferroquadrupolar order. This is in sharp contrast to the widely observed CE-type C/O order[22,23] and the related family of orbitally-striped phases,[24–26] in which the stripes lie parallel to $\langle 110\rangle$ directions and produce transverse, rather than longitudinal, displacements. The CE-type C/O configurations support alternating rows of Mn^{4+} and Mn^{3+} sites as well as alternating $d(3x^2-r^2)$ and $d(3y^2-r^2)$ orbitals (i.e., charge+antiferroquadrupolar order), so as to minimize both Coulomb and lattice-strain energies.[22,23,27] Second, the modulation in Fig. 3 indicates a smoothly varying charge density. Small Jahn-Teller polaron models involve discrete Mn^{3+} and Mn^{4+} valence states, such that the $Mn^{3+}O_6$ octahedra are strongly distorted, while the $Mn^{4+}O_6$ octahedra retain their symmetry. The modulation satellites in $La_{1.2}Sr_{1.8}Mn_2O_7$ are quite broad, but still much too narrow to be explained as an incoherent sum of scattering from distinct regions with commensurate modulation periods such as $3\boldsymbol{a}$ and $4\boldsymbol{a}$. The incommensurate nature of the periodic Jahn-Teller distortions in Figure 3 indicates an e_g electron density that varies continuously across the lattice within the 25 Å correlated regions, resulting in MnO_6 octahedra with mixed Mn^{3+}/Mn^{4+} characteristics. And if the amplitude of the charge density modulation is weak, the valence endpoints of the modulation will not be exactly $3+$ and $4+$. Assuming that the average valence is dictated by the composition, a simple bond-valence sum analysis[28,29] based on Table I yields valence end points of 3.4 ± 0.1 Note that this amplitude is roughly proportional to the maximum oxygen displacement assumed, and quite small, even for larger displacements.

A single-crystal neutron-diffraction study of long-range CE-type C/O order at $x=0.5$ concluded that the Jahn-Teller-distortions observed[20] in $LaSr_2Mn_2O_7$ were also too small to be explained in terms of discrete $3+$ and $4+$ valence states. The smooth modulation of its charge and orbital degrees of freedom were instead interpreted as a weak charge-density wave (CDW) with $\mathbf{q}_{CE}=(1/4,1/4,0)$. Short-range CDW fluctuations are common in a variety of low-dimensional systems, where they occur over an extended temperature range above a three-dimensional ordering temperature, and give rise to diffuse reciprocal-space streaks similar to the diffuse peaks[30] seen in Fig. 1. Their formation generally requires a peak in the electronic susceptibility at the CDW wave vector, usually a result of Fermi-surface nesting, together with strong electron-phonon coupling, which then permits a structural modulation to lift the nesting-related degeneracy.[31] Furthermore, the 180° interlayer phase difference observed in Fig. 3 is a common feature[31] of layered CDW systems that exhibit weak electron hopping between layers, which slightly corrugates the nested Fermi surfaces and thereby shifts the nesting condition by $q_z=\pm1$. In the case of $La_{1.2}Sr_{1.8}Mn_2O_7$, the modulation wave vector does appear to be related to the electronic structure, as recent angle-resolved photoemission spectroscopy measurements and density-functional calculations reveal pronounced Fermi-surface nesting features in the metallic phase below T_c, with nesting vector $2\mathbf{q}_F\approx(0.3,0,\pm1)$, while a wide pseudogap is observed to open above T_c.[32,33] The long-range strain fields that produce the anisotropic butterfly scattering of Fig. 1 provide another important means of imposing nanoscale structure within the polaronic state. Because these strain fields overlap in e_g electron-rich $La_{1.2}Sr_{1.8}Mn_2O_7$, a $\mathbf{q}$ dependence in the resulting strain-mediated interpolaron interactions would also be expected to contribute to the structural modulation.

IV. CONCLUSION

Rather than hosting independent polarons, an approximation that may be valid at low hole doping, the CMR manganites possess a dense population of polarons that interact via overlapping strain fields and electronic wave functions, and might be described as polaronic liquids. The $\mathbf{q}\approx(0.3,0,\pm1)$ modulation uncovered in the present analysis is structurally consistent with a Jahn-Teller-coupled charge-density-wave fluctuation and possesses a plausible connection to Fermi-surface nesting features reported below T_c. A longitudinal modulation of this nature has not been observed in the three-dimensional CMR manganites, and may be unique to layered systems where the lower dimensionality greatly enhances the fraction of the Fermi surface that can be nested. Yet, much remains to be discovered about the extent to which the $\mathbf{q}$ dependence of the strain-mediated interpolaron interactions and the electronic susceptibility of the adjacent ferromagnetic metallic state play a role in its development. The complex nanoscale structure within the polaronic state of $La_{1.2}Sr_{1.8}Mn_2O_7$ presents a challenge to our understanding and warrants further theoretical and experimental investigation into the nature of a concentrated population of strongly interacting polarons.

ACKNOWLEDGMENTS

This work was supported by the U.S. DOE Office of Science under contract W-31-109ENG-38 and by the State of

Illinois under HECA. We also acknowledge Václav Petříček (Institute of Physics AVCR, Czech Republic) for useful insights and assistance with the JANA software, James Phillips (Bruker-AXS, Madison, WI) for assistance with the CCD camera, and J. C. Lang (SRI-CAT, Advanced Photon Source) for technical assistance at the 1ID beamline, as well as Richard Klemm, Michael Norman, and Dan Dessau for helpful discussions.

*Electronic address: branton@anl.gov

[1] A.J. Millis, P.B. Littlewood, and B.I. Shraiman, Phys. Rev. Lett. **74**, 5144 (1995).
[2] A.J. Millis, R. Mueller, and B.I. Shraiman, Phys. Rev. B **54**, 5405 (1995).
[3] C. Zener, Phys. Rev. **82**, 403 (1951).
[4] K. Kubo and N. Ohata, J. Phys. Soc. Jpn. **33**, 21 (1972).
[5] H. Röder, J. Zang, and A.R. Bishop, Phys. Rev. Lett. **76**, 1356 (1996).
[6] A.A.Y. Tomioka, Y. Moritomo, and Y. Tokura, J. Phys. Soc. Jpn. **64**, 3626 (1995).
[7] S.J.L. Billinge, R.G. DiFrancesco, G.H. Kwei, J.J. Neumeier, and J.D. Thompson, Phys. Rev. Lett. **77**, 715 (1996).
[8] L. Vasiliu-Doloc, S. Rosenkranz, R. Osborn, S.K. Sinha, J.W. Lynn, J. Mesot, O.H. Seeck, G. Preosti, A.J. Fedro, and J.F. Mitchell, Phys. Rev. Lett. **83**, 4393 (1999).
[9] M. Kubota, Y. Oohara, H. Yoshizawa, H. Fujioka, K. Shimizu, K. Hirota, Y. Moritomo, and Y. Endoh, J. Phys. Soc. Jpn. **69**, 1986 (2000).
[10] S. Shimomura, N. Wakabayashi, H. Kuwahara, and Y. Tokura, Phys. Rev. Lett. **83**, 4389 (1999).
[11] C.P. Adams, J.W. Lynn, Y.M. Mukovskii, A.A. Arsenov, and D.A. Shulyatev, Phys. Rev. Lett. **85**, 3954 (2000).
[12] P. Dai, J.A. Fernandez-Baca, N. Wakabayashi, E.W. Plummer, Y. Tomioka, and Y. Tokura, Phys. Rev. Lett. **85**, 2553 (2000).
[13] K. Huang, Proc. R. Soc. London, Ser. A **190**, 102 (1947).
[14] V. Petříček and M. Dušek, *JANA2000* (Institute of Physics, Praha, Czech Republic, 2000).
[15] A. Yamamoto, Acta Crystallogr., Sect. A: Found. Crystallogr. **52**, 509 (1996).
[16] T. Janssen, A. Janner, A. Looijenga-Vos, and P.M. de Wolff, in *International Tables for Crystallography*, 2nd ed., edited by A.J.C. Wilson and E. Prince (Kluwer Academic, Dordrecht, Boston, London, 1999), Vol. C.
[17] Because the diffuse satellites are located adjacent to the $h+k+l=2n+1$ positions, $(h,k)=(o,e)$ not only indicates that h is odd and k is even, but also implies that l is even.
[18] V. Petříček and P. Coppens, Acta Crystallogr., Sect. A: Found. Crystallogr. **44**, 1051 (1988).
[19] The average atomic coordinates were taken from refinements of the parent $I4/mmm$ structure at 125 K using neutron powder-diffraction data. An overall isotropic thermal parameter was set to 0.002 Å. See related work: J.F. Mitchell *et al.*, Phys. Rev. B **55**, 63 (1997); M. Medarde *et al.*, Phys. Rev. Lett. **83**, 1223 (1999).
[20] D.N. Argyriou, H.N. Bordallo, B.J. Campbell, A.K. Cheetham, D.E. Cox, J.S. Gardner, K. Hanif, A. dos Santos, and G.F. Strouse, Phys. Rev. B **61**, 15 269 (2000).
[21] T. Kimura, R. Kumai, Y. Tokura, J.Q. Li, and Y. Matsui, Phys. Rev. B **58**, 11 081 (1998).
[22] E.O. Wollan and W.C. Koehler, Phys. Rev. **100**, 545 (1955).
[23] J.B. Goodenough, Phys. Rev. **100**, 564 (1955).
[24] C.H. Chen, S.-W. Cheong, and H.Y. Hwang, J. Appl. Phys. **81**, 4326 (1997).
[25] S. Mori, C.H. Chen, and S.-W. Cheong, Nature (London) **392**, 473 (1998).
[26] P.G. Radaelli, D.E. Cox, L. Capogna, S.-W. Cheong, and M. Marezio, Phys. Rev. B **59**, 14 440 (1999).
[27] T. Mutou and H. Kontani, Phys. Rev. Lett. **83**, 3685 (1999).
[28] R.D. Shannon and C.T. Prewitt, Acta Crystallogr., Sect. B: Struct. Crystallogr. Cryst. Chem. **25**, 925 (1969).
[29] N.E. Brese and M. O'Keeffe, Acta Crystallogr., Sect. B: Struct. Sci. **47**, 192 (1991).
[30] J.P. Pouget and R. Comes, in *Charge Density Waves in Solids*, edited by L.P. Gor'kov and G. Grüner (North-Holland, Amsterdam, 1989), Chap. 3.
[31] G. Grüner, *Density Waves in Solids* (Perseus, Cambridge, MA, 1994), Chap. 1.
[32] T. Saitoh, D.S. Dessau, Y. Moritomo, T. Kimura, Y. Tokura, and N. Hamada, Phys. Rev. B **62**, 1039 (2000).
[33] Y.-D. Chuang, A.D. Gromko, D.S. Dessau, T. Kimura, and Y. Tokura, Science **292**, 1509 (2001).